

Fragile \mathcal{PT} –symmetry in a solvable model

Miloslav Znojil¹

Ústav jaderné fyziky AV ČR, 250 68 Řež, Czech Republic

Abstract

One of the simplest pseudo-Hermitian models with real spectrum (viz., square-well on a real interval \mathcal{I} of coordinates) is re-examined. A \mathcal{PT} –symmetric complex deformation \mathcal{C} of \mathcal{I} is introduced and shown tractable via an innovated approach to matching conditions. The result is surprising: an *arbitrarily small* deformation $\mathcal{I} \rightarrow \mathcal{C}$ implies a sudden collapse (i.e., the spontaneous \mathcal{PT} –symmetry breaking) of virtually *all* the spectrum (i.e., up to its low-energy part).

PACS 03.65.Fd

¹e-mail: znojil@ujf.cas.cz

1 Non-Hermitian Hamiltonians and their spectra

Thirty five years ago, Bender and Wu [1] published an extremely exciting discovery that certain bound-state problems may be much better understood when one drops the “obligatory” Hermiticity assumption $H = H^\dagger$ and admits that a coupling constant $g > 0$ in Schrödinger equation

$$H(g) |\psi_n(g)\rangle = E_n(g) |\psi_n(g)\rangle, \quad n = 0, 1, \dots \quad (1)$$

is analytically continued to a complex value $g \in \mathbb{C}$. In this perspective Bender and Wu worked, for definiteness, with the quartic anharmonic-oscillator Hamiltonians

$$H(g) = H^{(4)}(g) = \hat{p}^2 + f^2 \hat{x}^2 + g \hat{x}^4, \quad (2)$$

and demonstrated that the separate (though, in general, complex) spectra $\{E_n(g)\}$ may *all* be interpreted as the sets of an intersection of *all* the Riemann sheets of a *single* analytic function $\mathbb{E}^{(4)}(g)$ with a corresponding “line” of a constant g . Many years later, similar observations were made and verified for the cubic model

$$H(g) = H^{(3)}(g) = \hat{p}^2 + f^2 \hat{x}^2 + i g \hat{x}^3 \quad (3)$$

(see the review [2] for more details) etc. In all of these models, the costs of the generalization $H \neq H^\dagger$ proved much lower than expected. For all the nonzero couplings $g \neq 0$, all of their complex “exceptional points” (EP) [3] proved well separated in the complex plane of g for both $m = 4$ and $m = 3$.

A new important development of the subject emerged cca six years ago when Bender and Boettcher published their letter [4]. Having extended their attention to the whole class of the power-law models

$$H(g) = H^{(2+\delta)}(g) = \hat{p}^2 + f^2 \hat{x}^2 + g \hat{x}^2 (i \hat{x})^\delta, \quad \delta > 0, \quad g > 0 \quad (4)$$

[reproducing the above special cases (2) and (3) at $\delta = 2$ and $\delta = 1$, respectively], they summarized several existing perturbative and numerical experiments (for illustration one could cite, e.g., [5, 6, 7]), complemented them by numerous new WKB arguments and conjectured that after one introduces a suitable Hilbert space, *all* the Hamiltonians (4) (with, for simplicity, $f = 0$) will possess the *purely real* (and discrete and, from below, bounded, i.e., “observable-like”) spectra, in spite of their *manifestly* non-Hermitian origin.

For the pioneering conjecture of this type, several rigorous proofs {cf., e.g., the Fourier-transformation results [7] for eq. (2) at $g < 0$, or the manifest reality of perturbative energies after re-summation for eq. (3) at the real g [5]} were already available and many other had only to come {cf., for illustration, proofs in the difficult case of eq. (3) in [8]}. Nevertheless, the core of the message delivered by Bender and Boettcher lied in the emphasis attributed to the parity-plus-complex-conjugation symmetry (conveniently called \mathcal{PT} -symmetry) of their sample non-Hermitian Hamiltonians $H^{(2+\delta)}(g)$ with real spectra. This inspired an extensive subsequent study of the structure of the relationship between the reality of the spectrum and the \mathcal{PT} -symmetry of the underlying non-Hermitian Hamiltonian [9].

We intend to contribute to the latter effort by the description of an exactly solvable example which exhibits a rather counterintuitive enhanced sensitivity to a very small change of its coordinate domain. We shall start from an overall review of the state of the art in section 2 where we emphasize the theoretical importance as well as some practical weaknesses of the pseudo-Hermitian constraint imposed upon the non-Hermiticity of the Hamiltonians.

In the next section 3 we return to the study of quantitative characteristics of the specific, differential-equation models where the current and robust property of Hermiticity $H = H^\dagger$ is being replaced by the \mathcal{PT} -symmetry which may be fragile [10, 11]. We restrict our attention to the most elementary non-Hermitian square-well model (of ref. [12], with real spectrum) and extend its scope slightly by the replacement of its usual domain (viz., a finite interval \mathcal{I}) by a broken line (or by any other smoothly deformed curve \mathcal{C} - cf. Figure 1) in the complex plane of coordinates.

Our main mathematical results are presented in section 4 where our new method of solving the matching conditions is shown applicable to an explicit qualitative description of the structure of the bound states in the broken-path regime. We explain in detail how our “moving-lattice” method decisively facilitates the global analysis of the matching conditions.

Our key physical message is finally formulated in section 5 emphasizing that our innovative geometric interpretation of the matching conditions offers the rigorous proof that in our example, an arbitrarily small imaginary shift $0 \rightarrow i\omega$ of the matching point causes a non-perturbative, *sudden* complexification of *all* the high-energy part of the spectrum. In the currently accepted terminology this means that the vast majority of the wavefunctions encounters a spontaneous breakdown of *their*

\mathcal{PT} -symmetry. We shall conclude in section 6 that this symmetry is *manifestly* fragile in our particular model.

2 \mathcal{PT} -symmetry

2.1 Variational picture

In the early stages of study of \mathcal{PT} -symmetric quantum mechanics people tried to understand the complexified Schrödinger Hamiltonians of the type (4) as models on the real line, with a pair of the real and imaginary potentials of a definite behaviour with respect to the parity \mathcal{P} . Along these lines one arrives at an introduction of the two harmonic-oscillator-type bases $\{|n^{(\pm)}\rangle\}$ (with definite, fixed parities $^{(\pm)}$) and transforms the \mathcal{PT} -symmetric differential Schrödinger equations $H|\psi\rangle = E|\psi\rangle$ with a pre-selected normalization of $|\psi\rangle = \sum_n (|n^{(+)}\rangle\psi_n^{(+)} + i|n^{(-)}\rangle\psi_n^{(-)})$ into the variational-like real and partitioned matrix problems containing arrays $\vec{\psi}^{(\pm)}$ of the real wavefunction components $\psi_n^{(\pm)}$,

$$\begin{pmatrix} A & -C \\ C^T & D \end{pmatrix} \begin{pmatrix} \vec{\psi}^{(+)} \\ \vec{\psi}^{(-)} \end{pmatrix} = E \begin{pmatrix} \vec{\psi}^{(+)} \\ \vec{\psi}^{(-)} \end{pmatrix}. \quad (5)$$

The infinite-dimensional submatrices $A = A^T$ and $D = D^T$ are real and symmetric but the spectrum itself need not be real at all [13]. These considerations inspired Mostafazadeh who conjectured, in a series of papers [14], that the Bender's and Boettcher's \mathcal{PT} -symmetric quantum mechanics should be classified as a mere special case of the more universal pseudo-Hermitian quantum mechanics, the origins and foundations of which might be traced back to Dirac et al [15]. In such an overall setting, he proposed to weaken the \mathcal{PT} symmetry of the Hamiltonians to their mere pseudo-Hermiticity

$$H^\dagger = \eta H \eta^{-1}, \quad \eta = \eta^\dagger \quad (6)$$

where we may set, in our particular example (5),

$$\eta = \eta_{\mathcal{P}} = \begin{pmatrix} I & 0 \\ 0 & -I \end{pmatrix} = \eta_{\mathcal{P}}^{-1}. \quad (7)$$

In the light of the well known [16] huge ambiguity of the assignment of the “metric” η to any given pseudo-Hermitian Hamiltonian $H \neq H^\dagger$, Mostafazadeh also proposed that the “natural” choices with the indeterminate parity-like metric operators [like

$\eta_{\mathcal{P}}$ in eq. (7)] should be *all* replaced by *any* (i.e., very often, non-diagonal and strongly Hamiltonian-dependent) positive definite alternative $\eta_+ > 0$. In parallel to Mostafazadeh, similar conclusions have been reached in refs. [17] and [18] defining, in the present language, the particular positive definite metrics $\eta_+ = \mathcal{P}\mathcal{Q}$ and $\eta_+ = \mathcal{C}\mathcal{P}$ using the additional symmetry generators \mathcal{Q} and \mathcal{C} of quasi-parity and charge, respectively.

The latter procedure enables us to call all the similar non-Hermitian Hamiltonians H “quasi-Hermitian” because, in accord with the review [16], the positivity of $\eta_+ > 0$ suppresses many interpretation difficulties and leaves the quasi-norm $\|\varphi\| = \sqrt{\langle \varphi | \eta_+ | \varphi \rangle}$ real and non-degenerate. This makes the corresponding Hamiltonians compatible with their standard quantum-mechanical probabilistic tractability [19].

2.2 Square-well illustration

One of the main sources of inspiration for the selection of potentials in Schrödinger equations (say, in the Coulombic form) is the principle of correspondence which allows us to extend and transfer to quantum mechanics the experimental experience gained during centuries in the common, macroscopic world. A counterintuitive character of many quantum phenomena allows us to search for some new and unusual Schrödinger equations, e.g., by a complexification of their axes of coordinates $\mathbb{R} \rightarrow \mathbb{C}$ [4]. Alternatively, we may obtain manifestly \mathcal{PT} -symmetric equations

$$\left[-\frac{d^2}{dx^2} + V(x) + iW(x) \right] \psi(x) = E \psi(x) \quad (8)$$

by staying on the real line and “deforming” the shapes of $V(x) = +V(-x)$ and $W(x) = -W(-x)$. Samples of both these approaches may be found, e.g., in ref. [10] (considering mainly the asymptotically power-law potentials) or [20] (paying attention to some exponentially confining forces) or [12] (where an even steeper, infinitely deep square well has been complexified) or [21] (where the mathematical properties have been discussed for the next-step models with delta-functions mimicking the “infinitely thin” square wells). The square-well model represents a reasonable phenomenological compromise exhibiting, as a bonus, an important merit of exact solvability. We shall pick up it in what follows, interpreting the infinitely deep real

part of the potential

$$V(x) = \begin{cases} +\infty & x > 1 \\ 0 & -1 < x < 1 \\ +\infty & x < -1 \end{cases} \quad \text{for} \quad \begin{cases} x > 1 \\ -1 < x < 1 \\ x < -1 \end{cases} \quad (9)$$

as a requirement that all the wavefunctions vanish at $x = \pm 1$. We break the Hermiticity of our Hamiltonian by adding the imaginary and \mathcal{PT} -symmetric finite interaction term with coupling $Z > 0$,

$$W(x) = \begin{cases} +iZ, & \text{for } \begin{cases} \text{Re } x < 0 \\ \text{Re } x > 0 \end{cases} \\ -iZ \end{cases} \quad (10)$$

Once we assume that the interval of the coordinates x remains purely real, the spectrum of energies $E_n = E_n(Z)$ proves discrete and real at all $Z < Z_{critical} \approx 4.48$ (cf. ref. [22]). It smoothly converges towards the well known square-well energy levels $E_n(0) = (n+1)^2\pi^2/4$ in the Hermitian limit $Z \rightarrow 0$.

In an extension of the above square-well model we shall now assume that the interval of the coordinates x is deformed to complex plane. The corresponding generalized, \mathcal{PT} -symmetric (i.e., left-right-symmetric) curve \mathcal{C} is sampled in Figure 1.

3 Exact solvability of the new model

Once we define our potential (10) in the whole complex plane of $x \in \mathcal{C}$, solutions $\psi(x)$ will be analytic in both its half-planes. The only distinctive feature of our present generalization $(-1, 1) = \mathcal{I} \rightarrow \mathcal{C}$ lies in the requirement of the matching of the left and right branches $\psi_{\mp}(x)$ of our full wavefunction $\psi(x)$ at a point $x_0 = i\omega$ on the imaginary axis. This enables us to postulate the matching rules

$$\psi_{-}(i\omega) = \psi_{+}(i\omega) = 1, \quad \partial_x \psi_{-}(i\omega) = \partial_x \psi_{+}(i\omega) = iA \quad (11)$$

in terms of an auxiliary real parameter $A \in (-\infty, \infty)$.

3.1 Re-parametrization of the matching conditions

As long as our potentials V and W are constant almost everywhere, the general solution of our differential Schrödinger equation (8) may be put equal to a sum of

the hyperbolic sine and cosine. The left and right solutions $\psi_{\mp}(x)$ are different, having to vanish at the different boundary points $x \rightarrow \mp 1$,

$$\psi_{-}(x) = R_{-} \sinh \kappa^{*}(1+x), \quad \psi_{+}(x) = R_{+} \sinh \kappa(1-x). \quad (12)$$

With $\kappa = s - it$, the values of the two free real parameters s and t will be determined by the differentiation in eq. (8),

$$E = t^2 - s^2, \quad Z = 2st. \quad (13)$$

As long as a change of the sign of κ would influence just the (arbitrary) sign of the overall normalization coefficients R_{\pm} , we conveniently restrict our attention to the quadrant of $s > 0$ and $t > 0$ (note that we fixed the sign of $Z > 0$ in advance). The insertion of the right and left solutions (12) in the matching conditions (11) gives the following complex (and transcendental) algebraic equations,

$$L \sinh \kappa^{*}(1+i\omega) = R \sinh \kappa(1-i\omega) = 1,$$

$$\kappa^{*} L \cosh \kappa^{*}(1+i\omega) = -\kappa R \cosh \kappa(1-i\omega) = iA.$$

Their solution is our main task. In the first step, we can get rid of the redundant constants by taking the ratios,

$$\kappa^{*} \coth \kappa^{*}(1+i\omega) = -\kappa \coth \kappa(1-i\omega) = iA. \quad (14)$$

The former equal sign is trivial while the latter one represents a complex equation which defines the real parameter A and inter-relates the two real and positive parameters s and t in addition. As long as we have $Z = 2st$, this should determine all their admissible values.

Changing our notation and putting $\omega = \tan \varphi$ with $\varphi \in (-\pi/2, \pi/2)$, let us now introduce two auxiliary linear functions $S = S(s, t)$ and $T = T(s, t)$ defined by the elementary two-dimensional rotation

$$\begin{pmatrix} S \\ T \end{pmatrix} = \begin{pmatrix} \cos \varphi & -\sin \varphi \\ \sin \varphi & \cos \varphi \end{pmatrix} \begin{pmatrix} s \\ t \end{pmatrix} \quad (15)$$

where the angle of the rotation measures also the upward shift of the matching point in the complex plane of our complex coordinates. In this notation we may re-write our matching constraint (14) in the form

$$A \sinh \left(\frac{S}{\cos \varphi} - i \frac{T}{\cos \varphi} \right) = (t + is) \cosh \left(\frac{S}{\cos \varphi} - i \frac{T}{\cos \varphi} \right) \quad (16)$$

which admits a facilitated separation of its real and imaginary part. The value of A drops out of their ratio which may be further re-arranged to represent our matching condition in the most compact real form

$$s \sinh \left(\frac{2S}{\cos \varphi} \right) = -t \sin \left(\frac{2T}{\cos \varphi} \right). \quad (17)$$

In the limit $\varphi \rightarrow 0$ the latter equation coincides with the $\omega = 0$ prescription of ref. [12]. At the generalized $\omega \neq 0$ the replacement of s and t by S and T via eq. (15) converts our new and more complicated matching formula (17) into its final form

$$\tau = \sigma \frac{\omega + \varrho(\tau) \sinh \sigma}{1 - \varrho(\tau) \omega \sinh \sigma}, \quad \omega = \tan \varphi \quad (18)$$

where we abbreviated $\sigma = 2S/\cos \varphi$, $\tau = 2T/\cos \varphi$ and $\varrho = \varrho(\tau) = -1/\sin \tau$. This equation is an implicit definition of a certain set of curves $\tau = \Theta(\sigma)$ in the $\sigma - \tau$ plane. In principle, the knowledge of these curves would enable us to find all their intersections (σ_k, τ_k) , $k = 0, 1, \dots$ with our original constraint $t = Z/(2s)$.

3.2 The lattice-moving method of solving eq. (18)

Our present key idea is that the function $\varrho = \varrho(\tau)$ is periodic, i.e., it remains constant on a discrete lattice \mathcal{L} of its argument τ . In this spirit we shall split the real axis of τ into intervals of the length 2π numbered by an integer k . Then we introduce the second variable $p = \pm 1$ marking the right and the left half of each of these intervals, respectively. This guarantees that at a fixed p the sign of the sine function remains the same and equal to $-p$. Finally, due to the symmetry of each of the sine-shaped curves we split the half-intervals in the quarter-intervals marked by another index $q = \pm 1$,

$$\tau = (2k + 1) \pi + p \frac{\pi}{2} + q \frac{\pi}{2} \xi \equiv \tau_{(k,q)}(p, \xi), \quad \xi = \xi(\tau) \in (0, 1). \quad (19)$$

As a consequence, our parameters $\varrho(\tau)$ become represented by the functions which are independent of k and q ,

$$\Omega(p, \xi) = -\frac{1}{\sin \tau_{(k,q)}(p, \xi)} = +\frac{p}{\cos(\pi \xi/2)}. \quad (20)$$

This means that the parameters ϱ remain constant over all the lattices $\mathcal{L}_{(p_0, \xi_0)}$ of points $\tau_{(k,q)}(p_0, \xi_0)$ where the sign p_0 and the parameter ξ_0 are temporarily fixed.

3.2.1 Verification: Straight-path solution re-visited

At $\omega = 0$ and $\mathcal{C} = \mathcal{I}$, the use of the limiting, simplified version

$$\tau = \varrho(\tau) \sigma \sinh \sigma, \quad \omega = 0 \quad (21)$$

of our matching condition (18) leads to an enormous simplification of the construction performed in ref. [12]. There, severe difficulties originated from a strong and pronounced τ -dependence of the factor $\varrho = \varrho(\tau)$ which is a very quickly changing function of its argument τ . In our present setting, the discretization (19) enables us to fix the value of $\varrho = \Omega$ by reducing our attention from all the values of τ to their lattices $\mathcal{L}_{(p,\xi)}$. Treating them separately, one at a time, we only have to keep in mind the overall range of our real constants $\Omega(p, \xi) = p |\Omega(p, \xi)| = p \Omega(+1, \xi) \notin (-1, 1)$. This enables us to re-parametrize the matching condition (21),

$$\tau = \tau_{(k,q)}(p, \xi) = \Omega(p, \xi) \sigma \sinh \sigma, \quad p, \xi = \text{fixed}. \quad (22)$$

In the new language, the graph of the function $\Omega \sigma \sinh \sigma$ is a parabolic curve which is oriented up or down at the respective $p = +1$ and $p = -1$. As long as we are interested in the positive $\tau > 0$, we may discard $p = -1$ and fix $\tau = \tau_{(k,q)}(+1, \xi) > 0$ and $\varrho(\tau) = \Omega(p, \xi) = \Omega(+1, \xi) \geq 1$. The curves $\tau = \Omega(+1, \xi) \sigma \sinh \sigma \equiv \Theta_\xi(\sigma)$ then shrink in proportion to the growth of ξ , proceeding from their broadest $\xi = 0$ version (where $|\Omega| = 1$) via the narrowing parabolic curves until the degenerate single and upwards-oriented half-line in the limit $\xi \rightarrow 1$, i.e., $\Omega \rightarrow \infty$. This is illustrated in Figure 2 where the unlimited shrinking of the curves is sampled at $\xi = 0, 0.5, 0.9$ and $\xi = 0.99$.

When we zoom out a stripe of $\tau = \tau_{(k,q)}(p, \xi)$ at a fixed $k = 30$ in Figure 2, we get Figure 3. In the new Figure the variations of τ are determined solely by the changes of ξ and q which are sampled by a few horizontal lines. As long as the right-hand-side function $\Theta_\xi(\sigma)$ depends on both σ and ξ , equation (22) will be satisfied *only* at the points of intersection of each particular ξ -marked horizontal line with another particular, ξ -assigned parabolic curve. In this manner the points of intersection $(\sigma_{\xi_m}, \tau_{\xi_m})$ in Figure 3 sample the graphical solution of the matching condition (22). As long as we choose a fairly large stripe number $k = 30$, the parabolas of Figure 2 are represented by the almost straight and almost vertical lines in Figure 3. This makes the identification of all the intersections particularly easy. We see that the points of intersection form the horizontally prolate ovals, each of which being confined within

its $k = k_0$ and $p = +1$ stripe, and not exceeding the interior of the “maximal”, $|\Omega| = 1$ parabola. It is obvious that the horizontal lines (= lattices of τ) as well as the more or less vertical parabolas move smoothly with the growth of ξ . The resulting picture reproduces precisely our old graphical proof [12] of the existence of solutions at $\omega = 0$. Our present new discretization method appears to offer a feasible extension of this proof and analysis to $\omega \neq 0$.

4 Bound states at $\omega \neq 0$ in graphical representation

Once we wish to determine the spectrum of the square-well energies $E_n = t_n^2 - s_n^2$ at any $\omega \neq 0$, we have to find all the real values of $s = s_n$ and $t = t_n$ which satisfy *both* the constant-coupling constraint (13) *and* the matching condition (17). In the first step, let us re-express the former elementary hyperbolic-curve correlation $Z = 2st$ in the new variables σ and τ .

4.1 The Z –dependent hyperbolic-curve constraint

Rotation (15) implies that under the assumption $\omega > 0$ we have $\tau > 0$ while the sign of σ may be both positive and negative. Alternatively, the choice of $\omega < 0$ would imply that we must keep $\sigma > 0$ while the sign of τ is allowed to vary. This means that one of the two hyperbolas defined by the rule $Z = 2st$ may be discarded immediately. Of course, in our innovated notation we must describe these hyperbolas by the slightly less transparent rotated quadratic equation

$$\tau^2 + 2\tau\sigma \frac{\cos 2\varphi}{\sin 2\varphi} - \sigma^2 - \frac{4Z}{\sin 2\varphi \cos^2 \varphi} = 0. \quad (23)$$

At $\omega = \tan \varphi > 0$ it is easy to select the correct branch defined by the formula

$$\tau = \Xi(\sigma) = \frac{1}{2} \left(\omega - \frac{1}{\omega} \right) \sigma + \frac{1}{2} \sqrt{\left(\omega + \frac{1}{\omega} \right)^2 \sigma^2 + 4X^2}, \quad X^2 = \frac{4Z}{\sin 2\varphi \cos^2 \varphi}. \quad (24)$$

In parallel, at $\omega = \tan \varphi = -\tilde{\omega} < 0$ we must use the *different* formula

$$\sigma = \Upsilon(\tau) = \frac{1}{2} \left(\frac{1}{\omega} - \omega \right) \tau + \frac{1}{2} \sqrt{\left(\omega + \frac{1}{\omega} \right)^2 \tau^2 + 4Y^2}, \quad Y^2 = \frac{-4Z}{\sin 2\varphi \cos^2 \varphi}. \quad (25)$$

In the other words, we must treat the up and down shifts $i\omega$ of the matching point separately, reflecting the fact that we already broke the symmetry between the half-planes of coordinates $x \in \mathcal{C}$ by having chosen the positive coupling $Z > 0$ in advance.

4.2 The second, matching constraint

The application of the lattice-shifting technique of section 3.2 may be extended to both the positive and negative ω . The variable $\tau = \tau_{(k,q)}(p, \xi)$ remains represented by the same function of the interval selector k , of the two sign-variables $q = \pm 1$ and $p = \pm 1$ and of the continuous ξ varying in the compact interval $(0, 1)$.

4.2.1 Moving lattices

Let us now select $\omega > 0$ and keep the two auxiliary variables p and ξ fixed. This restricts the range of our variable τ to the lattice $\mathcal{L} = \mathcal{L}(p, \xi)$ where the function $\Omega = \Omega(p, \xi) = p/\cos(\pi\xi/2)$ remains constant. This leads to a decisive simplification of our matching condition (18),

$$\tau = \Theta_{(p,\xi)}(\sigma) = \sigma \frac{\omega + \Omega \sinh \sigma}{1 - \Omega \omega \sinh \sigma}, \quad p, \xi = \text{fixed}. \quad (26)$$

A typical graph of the function $\Theta_{(p,\xi)}(\sigma)$ at both $p = \pm 1$ and at the minimal $\xi = 0$ and/or $|\Omega| = 1$ is displayed in Figure 4. With respect to the growth of the lattice-characterizing parameter ξ from 0 to 1 it is trivial to see from eq. (26) that

- at $p = +1$ and $\sigma > 0$, the right branch of the well-shaped curve $\Theta_{(+1,\xi)}(\sigma) > 0$ is bounded by its perpendicular asymptote at $\sigma_\infty(\xi) = \text{arcsinh}(1/[\omega\Omega(+1, \xi)])$. With the growth of ξ and Ω it inadvertently moves to the left and in the limit of $\xi \rightarrow 1$ it coincides with the vertical half-axis V_{right} ($\sigma_\infty(1) = 0$);
- in parallel, the left branch of the same well moves upwards and coincides with its diagonal asymptote D_{left} in the same limit, $\lim_{\xi \rightarrow 1} \Theta_{(+1,\xi)}(\sigma) = -\sigma/\omega$;
- at $p = -1$ and $\sigma < -\sigma_\infty(\xi) < 0$, there exists another hyperbolic well sampled in Figure 4, with definition $\tau = \Theta_{(-1,\xi)}(\sigma)$ and asymptotes D_{left} and (ξ -dependent) A_{right} . With the growth of ξ this well moves downwards and to the right and coincides with the wedge formed by D_{left} and V_{right} at $\xi = 1$.

This geometric picture has several consequences. The most important one is that at the minimal $\xi = 0$ the curves of Figure 4 contain the initial points of all the ovals of the solutions in the manner indicated by the $\xi = 0$ point in Figure 3 above. With the growth of ξ the similar oval-shaped curves are then being formed at any ω .

4.2.2 Four families of half-ovals

In a continuing description of the structure of solutions of eq. (26) we must distinguish between the positive and negative σ . For $\sigma \geq 0$, the analysis is simpler since the ovals (or rather half-ovals) as sampled in Figure 3 at $\omega = 0$ can solely exist in the stripes with $p = +1$. With the growth of ξ they open their two $q = \pm 1$ branches to the left until they attain their maximal width and reach the boundaries of their stripes on the vertical axis V_{right} in the limit $\xi \rightarrow 1$.

At $\sigma < 0$ we have to parallel the above half-ovals by their $p = +1$ partners which start to open to the right at the leftmost curve with $\xi = 0$. They end their growth at $\xi = 1$ while touching the boundaries of their $p = +1$ stripes on the diagonal D_{left} .

In contrast to our above $\omega = 0$ exercise in section 3.2.1, the choice of $\sigma < 0$ admits the existence of another family of the half-ovals within the $D_{left} - V_{right}$ wedge. Of course, they can only exist within the stripes where $p = -1$ and in the domain of the sufficiently large $\tau \gtrsim \tau_0$ (i.e., at $k \geq k_{minimal}$) where they can originate on the curve $\tau = \Theta_{(-1,0)}(\sigma) \geq \tau_0$. In this domain they form the two subfamilies again, depending on whether they originated on the left or right branch of the $\xi = 0$ curve.

4.2.3 Two patterns of gluing the half-ovals

With the growth of ξ , the left half-ovals within the wedge $D_{left} - V_{right}$ open to the left, ending their growth at $\xi = 1$ in the intersections of the boundaries of their $p = -1$ stripes with the left diagonal straight line D_{left} . At these points these half-ovals meet their $p = +1$ partners so that in contrast to the $\omega = 0$ pattern (with a series of the separated and closed ovals – cf. their picture in ref. [12]), the resulting locus of the solutions forms a wavy, sine-like-shaped line which oscillates to the left and right and moves up to the left along the diagonal D_{left} . As long as this curve remains confined between its two envelopes $\Theta_{(\pm 1,0)}(\sigma)$, the asymptotic decrease of the amplitude of this wobbling is exponential. A schematic example of such a wavy curve appears in Figure 5.

In the same range of the sufficiently large τ , the second, similar wavy pattern is formed along the axis V_{right} . In exactly the same manner it results from the gluing of the right $p = -1$ half-ovals which open to the right and reach the line V_{right} where they find a continuation in the above-mentioned $p = +1$ half-ovals at $\sigma > 0$. In contradistinction to the previous case, the amplitude of the wobbling is asymptotically constant. Still, this fact alone is sufficient to exclude this branch from

further consideration because the $Z = 2st$ constraint is asymptotically a hyperbola with asymptotes at the angles $\varphi = \arctan \omega$ and $\varphi' = \arctan \omega - \pi/2$ with respect to the axis V_{right} .

In all the remaining domain of the not too large values of τ , just smooth perturbations occur of the $\omega = 0$ pattern of disconnected ovals. At $\omega > 0$ the height of the ovals exceeds the height of a single stripe. This is consistent with the fact that an inner part of the ovals lies within the $D_{left} - V_{right}$ wedge and must belong, therefore, to a $p = -1$ stripe. This also does not contradict to the steady decrease of the minimum of the graph of the curve $\Theta_{(-1,\xi)}(\sigma)$ since with the growth of ξ the solutions of eq. (26) start to exist in the lower and lower $p = -1$ stripes within the wedge. In this way, the resulting loci of solutions of eq. (26) are allowed to form the separate ovals in a fully consistent manner, indeed.

5 Energies

The ultimate goal of our considerations is achieved. We clarified that an optimal strategy of the determination of all the parameters $s = s_n$ and $t = t_n$ in the bound-state formula $E_n = t_n^2 - s_n^2$, $n = 0, 1, \dots$ is based on a suitable change of variables $(s, t) \rightarrow (\sigma, \tau)$ which merely re-scales and rotates the original hyperbolic constraint $Z = 2st$ and re-expresses all the real deformed-path square-well energies by the “rotated” formula

$$E = E_n(Z, \varphi) = \frac{1}{4} \left[(\tau_n^2 - \sigma_n^2) \cos 2\varphi - 2\sigma_n\tau_n \sin 2\varphi \right] \cos^2 \varphi. \quad (27)$$

This leads to a vital simplification of the matching of wavefunctions. In the real $\sigma - \tau$ plane, the construction of all the physical bound states (if any) is reduced to an identification of all the admissible parameters (σ_n, τ_n) with all the intersections of a certain pair of curves. One of them is the elementary Z -dependent hyperbola (the smooth curve in Figure 5). A sufficiently transparent graphical representation of the shape of the second one is more difficult and required in fact the greater portion of our previous text. This curve is sampled by its quickly oscillating asymptotic part in Figure 5.

5.1 A comment on asymmetry between $\omega > 0$ and $\omega < 0$

We mainly paid attention to the positive values of the shift $\omega > 0$ pertaining to the generic form of the family of the hyperbolae given by eq. (24). They are sampled by the smoother curve in Figure 5. The Figure also illustrates a generic pattern of the intersection of these hyperbolae with half-oval families confined within areas specified by their envelope curves exemplified in Figure 4.

We did not notice in section 4.2.1 that after reflection of Figure 4 with respect to the origin of coordinates σ and τ , its $p = -1$ and $p = +1$ envelope curves are mapped upon each other. This simplifies marginally the construction and follows from the invariance of eq. (26) *on the lattices* since the simultaneous replacements $\tau \rightarrow -\tau$ and $\sigma \rightarrow -\sigma$ are equivalent to $\Omega \rightarrow -\Omega$ while the latter change of sign merely means that we have to transform $p \rightarrow -p$.

We did not deduce, *ibidem*, that another simultaneous sign-change of $\sigma \rightarrow -\sigma$ and $\omega \rightarrow -\omega$ preserves the form of the original, lattice-independent matching condition (18). This is more important because at the negative $\omega = -\tilde{\omega} < 0$ we would be forced to replace the most complicated pattern of Figure 4 (where we always employ the positive $\tilde{\omega} = |\omega|$) by its left-right-reflected copy complemented by the corresponding correct hyperbolic branch of curve $Z = 2st$ in its alternative form (25). After the left-right mirroring transform it enables us to simplify the situation by returning to the original Figure 4 complemented by the trivially modified reflected hyperbola

$$\sigma = \Sigma(\tau) = \frac{1}{2} \left(\frac{1}{\tilde{\omega}} - \tilde{\omega} \right) \tau - \frac{1}{2} \sqrt{\left(\tilde{\omega} + \frac{1}{\tilde{\omega}} \right)^2 \tau^2 + 4Y^2}, \quad Y^2 = \frac{+4Z}{\sin 2\tilde{\varphi} \cos^2 \tilde{\varphi}}. \quad (28)$$

Hence, all what we have derived at the positive ω may *immediately* be transferred to the case where ω is negative, *without* changing the half-oval curves and with the mere addition of the second branch (28) of the hyperbola. In Figure 5 this would just mean a replacement of the upper hyperbola by its minus-sign partner. Of course, such an extension of the whole picture is essentially trivial and it need not be discussed separately at all.

5.2 The breakdown of \mathcal{PT} symmetry at high energies

Our construction of a closed form of the bound states is transparent and, undoubtedly, potentially useful. For the straight path \mathcal{C} with $\omega = \varphi = 0$ and for all the values of $Z > 0$ which are not too large, the square-well model already found interesting applications in the study of the spontaneous \mathcal{PT} -symmetry breaking at

the sufficiently large Z [22]. An even more important role of this model seems to have emerged within the supersymmetric quantum mechanics [23]. In all these and similar applications, our present results simply mean that all the changes caused by a shift of a small size $|\omega|$ remain smooth if and only if we do not move to the very high energies.

In contrast to that, an introduction of *any* non-vanishing shift ω changes the high-energy region completely and abruptly. In place of infinitely many real and positive energies $E_n(Z)$, $n = 0, 1, \dots$ which formed the complete spectrum at $\omega = 0$, the choice of *any* $\omega = \tan \varphi \neq 0$ makes the number of the real intersections (σ_n, τ_n) *finite*, $n = 0, 1, \dots, n_{\max}(Z, \varphi)$ with a certain maximal real energy at $n_{\max}(Z, \varphi) < \infty$. The mathematical foundation of this conclusion is almost trivial: Up to a finite number of exceptions, the energies may only be generated by the intersections in the domain of the large $\tau \gg 1$ where both the Z -dependent hyperbolas with $\omega > 0$ and $\omega = -|\omega| < 0$ have almost the same asymptotic representation,

$$\tau = -\frac{1}{|\omega|} \sigma \mp \frac{|X^2|}{(|\omega| + 1/|\omega|)\sigma} + \mathcal{O}(\sigma^{-3}), \quad \text{sign } \omega = \pm 1, \quad \sigma \ll -1. \quad (29)$$

This means that both of them share the dominant term (representing just the straight line of their common asymptote D_{left}) and approach this asymptote at an inverse-power rate from above or below, respectively (the former case is illustrated in Figure 5 displaying just the deviation from the asymptote).

The same asymptote D_{left} is further shared by both the upper and lower envelopes $\Theta_{(\mp 1, 0)}(\sigma)$ of the second, quickly wobbling curve. Nevertheless, from definition (26) we easily derive their leading-order asymptotic form

$$\tau = -\frac{1}{|\omega|} \sigma \mp \frac{|\omega| + 1/|\omega|}{\sinh \sigma} + \mathcal{O}(\sinh^{-2} \sigma), \quad \text{sign } \omega = \pm 1, \quad \sigma \ll -1. \quad (30)$$

This implies that the *quick, exponential* decrease of *both* the envelopes in eq. (30) *guarantees* that the wobbling line cannot have *any* real intersections with *neither* of the two hyperbolic Z -dependent curves (29) with their too slow, power-law rate of approach to the asymptote. This is illustrated in Figure 5 as a key message of the whole construction and implies that the number of the real energies remains finite at *any* non-vanishing $\omega \neq 0$ and Z . In the other words, infinitely many real energies which existed at $\omega = 0$ become “lost” and “dissolved” in complex conjugate pairs. This occurs precisely at the moment when (say, in Figure 5) the intersecting Z -dependent hyperbola moves (say, due to a slight increase of Z) to the top of

a particular half-oval (there, the two energies merge at a “Bender-Wu singularity” [1] or “exceptional point” [3]) and, in the next stage, separates from the half-oval completely (ref. [22] studied this type of a pairwise complexification of the square-well energies at $\omega = 0$ in more detail).

The disappearance of the real intersections of the two curves in Figure 5 occurs at any $Z \neq 0$ and implies that the \mathcal{PT} symmetry of our wavefunctions becomes broken at all the sufficiently large energies. In the other words, our initial choice of the form of the wavefunctions does not suddenly represent *all* the possible bound-state solutions. In a way discussed in full detail in our previous $\omega = 0$ study [22] this means that all the “missing” bound states must be sought in a certain more-parametric and manifestly \mathcal{PT} -symmetry-breaking form.

The only exception is encountered at $Z = 0$ where the message offered by Figure 5 is different because in the limit $Z \rightarrow 0$ the upper hyperbolic curve moves down and coincides *strictly* with the horizontal axis. This forces us to return to the very origin of our present construction and repeat all its steps under the new explicit postulate that $t = 0$. In this case, the kind reader may easily verify that the $Z = 0$ result *proves* in fact *independent* of the value of ω so that all the repeated $Z = 0$ and $\omega \neq 0$ (i.e., non-Hermitian though still \mathcal{PT} -symmetric) construction returns us back to the energies which *coincide* with the well known Hermitian square-well spectrum.

6 Summary

All our results are summarized in Table 1 which may be read, first of all, as an advertisement of our almost involuntary discovery of an extremely elementary and transparent new \mathcal{PT} -symmetric model with real energies (cf. the last line). On a more general level, the main item in the review Table 1 (viz., its last but one line) warns against all the non-critical intuition which might prove misleading in the realm of \mathcal{PT} symmetric models. In this sense, our results may be perceived as a non-numerical complement to numerical experiments of paper [10] where several “not entirely smooth” potentials clearly inclined towards a spontaneous \mathcal{PT} -symmetry breakdown at high energies.

On this background we believe that in the nearest future, attention will be re-attracted to the real role of non-analyticity in the \mathcal{PT} symmetric potentials and models, with inspiration by our present rigorous proof that any non-vanishing shift

of ω at $Z \neq 0$ makes the \mathcal{PT} -symmetry of our square-well model *suddenly* to break down. This breakdown involves infinitely many levels at once, i.e., it occurs in a way which seems characteristic for virtually all the exactly solvable *analytic* models [11, 24]. At the same time, the discontinuity of the breakdown might reflect its *non-analytic* origin, contrasting with the robust survival of the reality of spectra under path-deformations in many not too strongly singular analytic potentials [25].

We have seen that the square-well model is exceptional in representing a solvable laboratory which seems to lie on a very boundary between “robust” and “fragile” models with \mathcal{PT} -symmetry. In this sense, our present key message is encouraging since the geometric language of our innovated “moving-lattice” method proved extremely efficient and seems productive. Its former aspect becomes clear when we compare the $\omega = 0$ discussion here and in ref. [12], while its second property is still to be verified in the future.

Acknowledgment

Partially supported by GA AS in Prague, contract No. A 1048302.

Figure captions

Figure 1. Integration path \mathcal{C} with an upwards deformation $\omega > 0$

Figure 2. The lattice-dependent curve (22) with $p = +1$ at a few ξ

Figure 3. The oval-shaped matching constraint $\tau = \Theta(\sigma)$ in its ξ -discretization at $\omega = 0$ and $k = 30$

Figure 4. Two lattice-dependent functions $\tau = \Theta_{(p,0)}(\sigma)$ at $\omega = 0.06$

Figure 5. Damped oscillations of $\Theta(\sigma)$ vs. constraint $2st = Z$

Table captions

Table 1. Cardinalities $N^{(real)}$ and $N^{(complex)}$ of the square-well energies E with $\text{Im } E = 0$ and $\text{Im } E \neq 0$, respectively

Table 1: Cardinalities $N^{(real)}$ and $N^{(complex)}$ of the square-well energies E with $\text{Im } E = 0$ and $\text{Im } E \neq 0$, respectively

ω	Z	$N^{(real)}$	$N^{(complex)}$	comment
0	0	∞	0	Hermitian case
0	$0 < Z < 4.475\dots$	∞	0	\mathcal{PT} -symmetric case of ref. [12]
0	$4.475\dots < Z < 12.8015\dots$	∞	2	\mathcal{PT} -symmetry broken [22]
0	$Z_N < Z < Z_{N+1}$	∞	2N	\mathcal{PT} -symm. br. at $E < E_{crit}(N)$
$\neq 0$	$\neq 0$	finite	∞	\mathcal{PT} -symm. br. at $E > E_{crit}(Z, \omega)$
$\neq 0$	0	∞	0	new \mathcal{PT} -symmetric case

References

- [1] C. M. Bender and T. T. Wu, Phys. Rev. 184 (1969) 1231.
- [2] G. Alvarez, J. Phys. A: Math. Gen. 27 (1995) 4589.
- [3] C. Dembowski et al, Phys. Rev. Lett. 86 (2001) 787;
W. D. Heiss and H. L. Harney, Eur. Phys. J. D 17 (2001) 149.
- [4] C. M. Bender and S. Boettcher, Phys. Rev. Lett. 24 (1988) 5243.
- [5] E. Caliceti, S. Graffi and M. Maioli, Commun. Math. Phys. 75 (1980) 51.
- [6] D. Bessis, private communication (1992).
- [7] V. Buslaev and V. Grecchi, J. Phys. A: Math. Gen. 26 (1993) 5541.
- [8] P. Dorey, C. Dunning and R. Tateo, J. Phys. A: Math. Gen. 34 (2001) 5679;
K. C. Shin, Commun. Math. Phys. 229 (2002) 543.
- [9] cf. the most recent update of references in the dedicated issue of Czech. J. Phys. 54 (2004) 1 - 156.
- [10] C. M. Bender, S. Boettcher and P. N. Meisinger, J. Math. Phys. 40 (1999) 2201.
- [11] G. Lévai, Czech. J. Phys. 54 (2004) 77, with the fresh update of further references.

- [12] M. Znojil, Phys. Lett. A. 285 (2001) 7.
- [13] M. Znojil, What is PT symmetry? (arXiv: quant-ph/0103054v1) and
Conservation of pseudo-norm in PT symmetric quantum mechanics (arXiv:
math-ph/0104012).
- [14] A. Mostafazadeh, J. Math. Phys. 43 (2002) 205, 2814, 3944 and 6343.
- [15] P. A. M. Dirac, Proc. Roy. Soc. London A 180 (1942) 1;
W. Pauli, Rev. Mod. Phys. 15 (1943) 175;
A. Ramírez and B. Mielnik, Rev. Fis. Mex. 49S2 (2003) 130.
- [16] F. G. Scholtz, H. B. Geyer and F. J. W. Hahne, Ann. Phys. (NY) 213 (1992)
74.
- [17] M. Znojil, Phys. Lett. A 259 (1999) 220 and 264 (1999) 108.
- [18] C. M. Bender, D. C. Brody and H. F. Jones, Phys. Rev. Lett. 89 (2002) 270401.
- [19] A. Mostafazadeh, Czech. J. Phys. 53 (2003) 1079;
C. M. Bender, Czech. J. Phys. 54 (2004) 13.
- [20] F. Fernández, R. Guardiola, J. Ros and M. Znojil, J. Phys. A: Math. Gen. 32
(1999) 3105.
- [21] S. Albeverio, S. M. Fei and P. Kurasov, Lett. Math. Phys. 59 (2002) 227;
M. Znojil, J. Phys. A: Math. Gen. 36 (2003) 7639.
- [22] M. Znojil and G. Lévai, Mod. Phys. Lett. A 16 (2001) 2273.
- [23] B. Bagchi, S. Mallik and C. Quesne, Mod. Phys. Lett. A17 (2002) 1651.
- [24] G. Lévai and M. Znojil, J. Phys. A: Math. Gen., 33 (2000) 7165.
- [25] M. Znojil, J. Phys. A: Math. Gen. 34 (2001) 9585;
V. Jakubský, Czech. J. Phys. 54 (2004) 67.

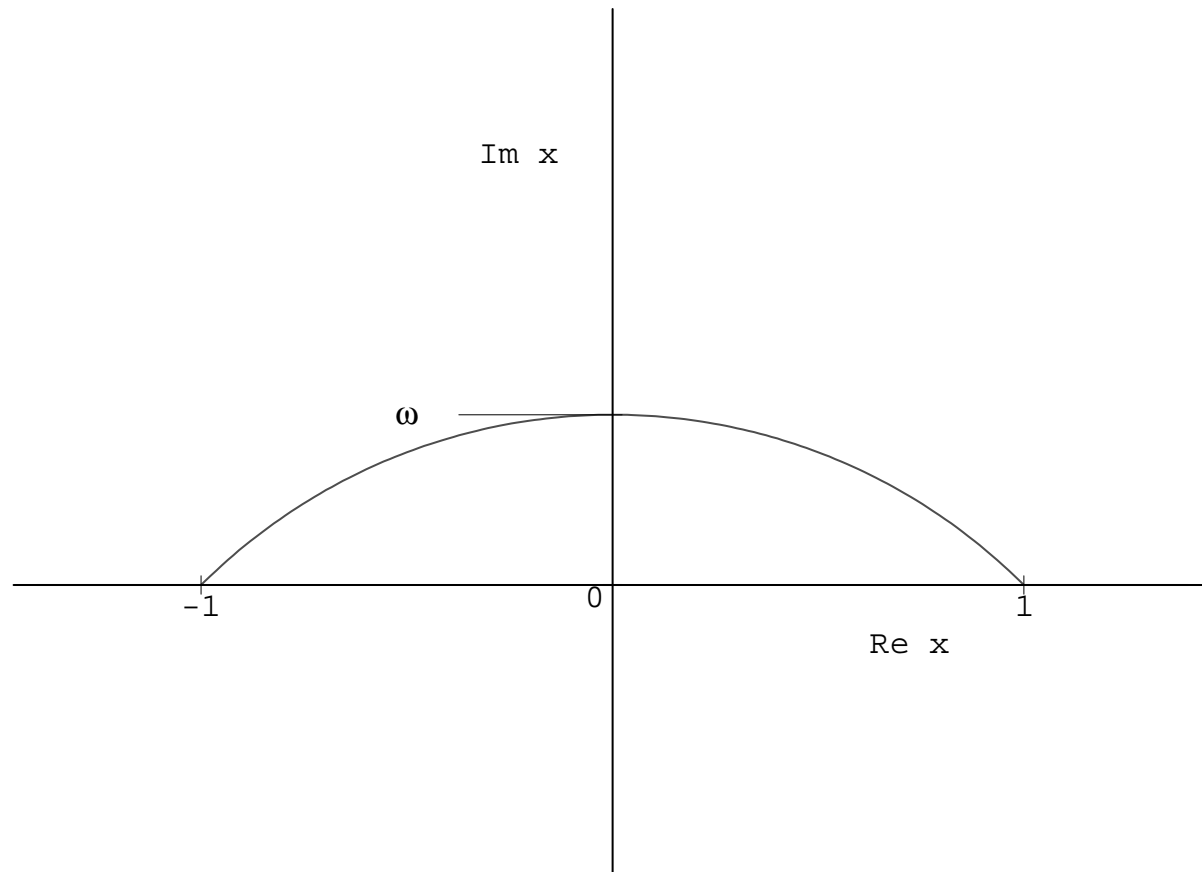


Figure 1. Integration path C
with an upwards deformation $\omega > 0$

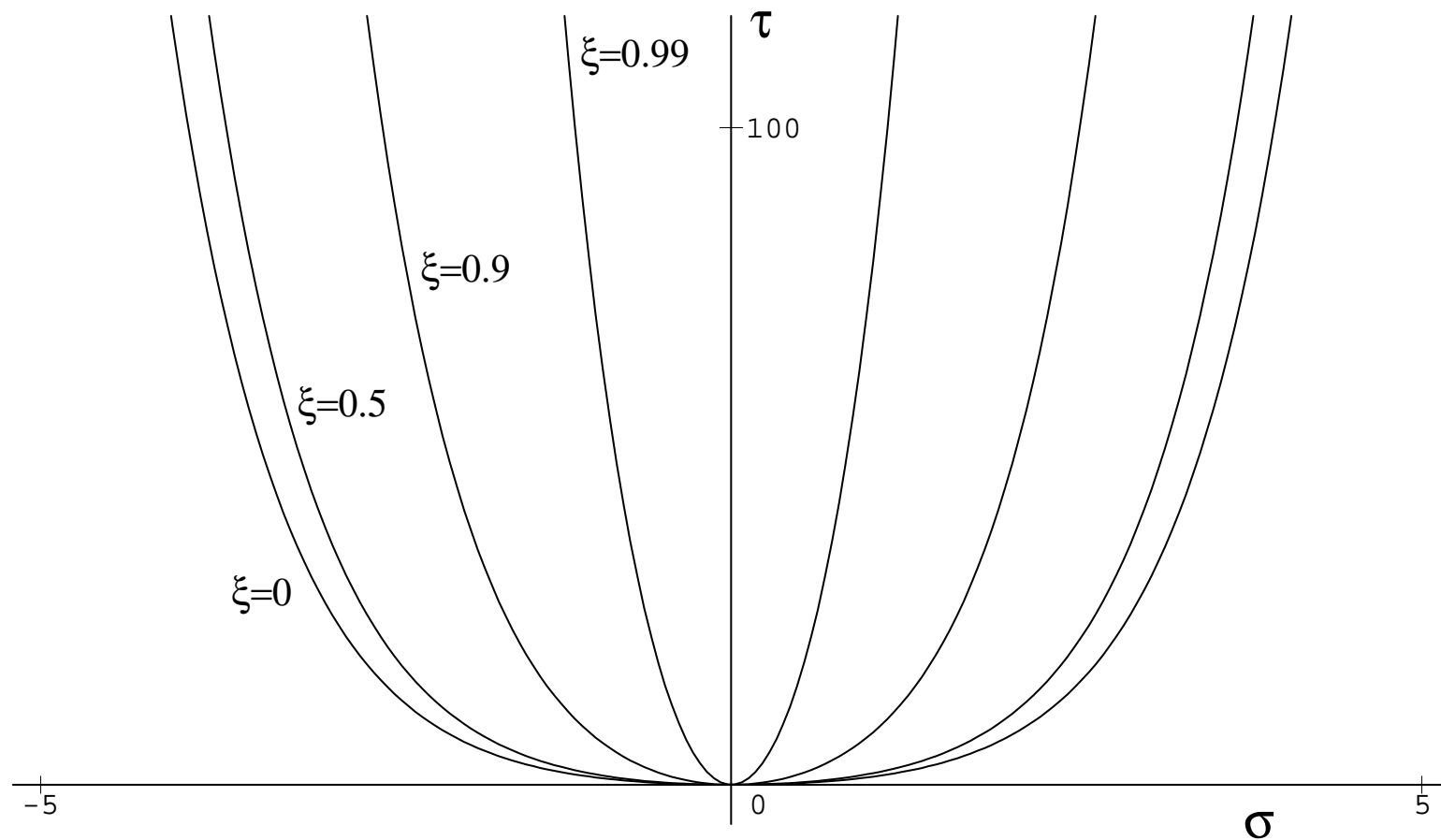


Figure 2. The lattice-dependent curve (24)
with $p=+1$ at a few ξ

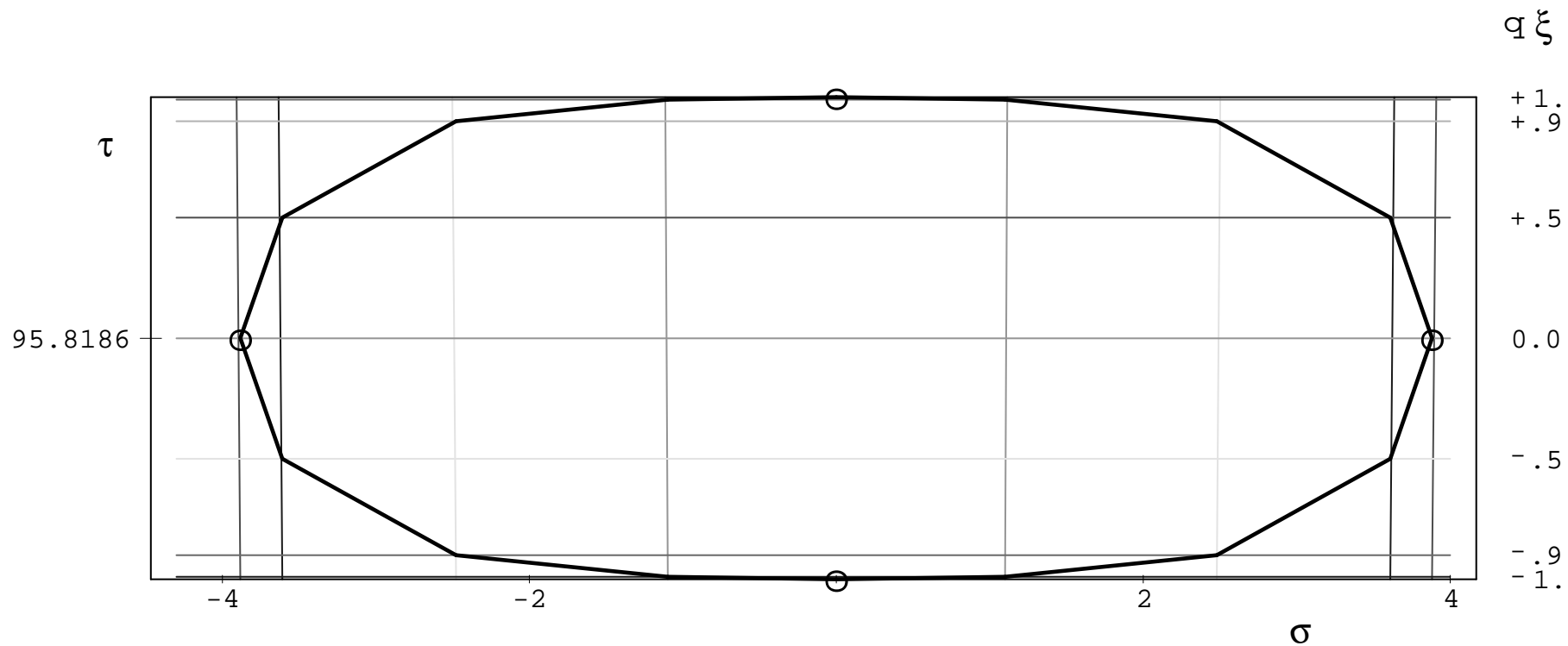


Figure 3. The oval-shaped matching constraint $\tau = \Theta(\sigma)$ in its ξ -discretization at $\omega=0$ and $k=30$

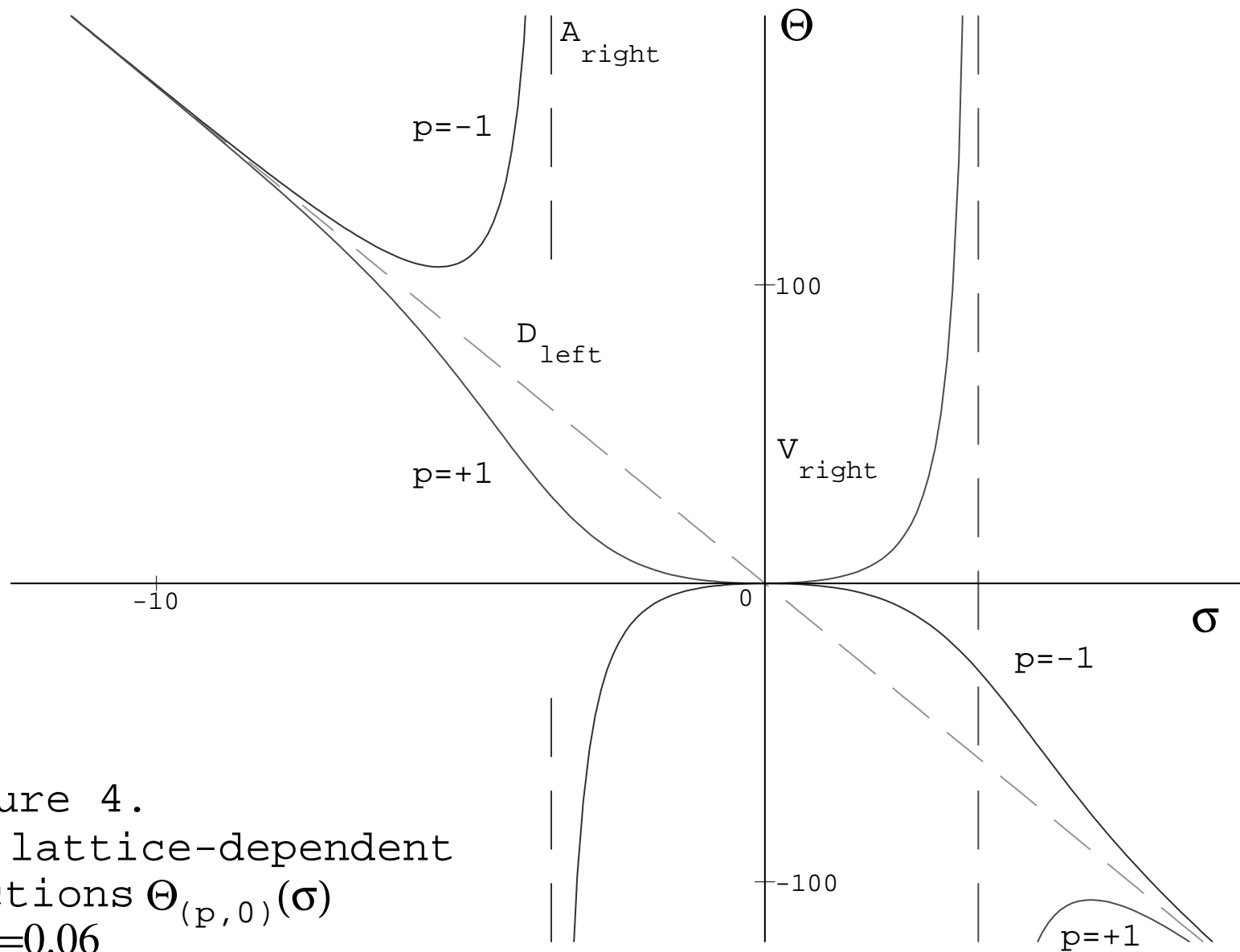


Figure 4.
Two lattice-dependent
functions $\Theta_{(p,0)}(\sigma)$
at $\omega=0.06$

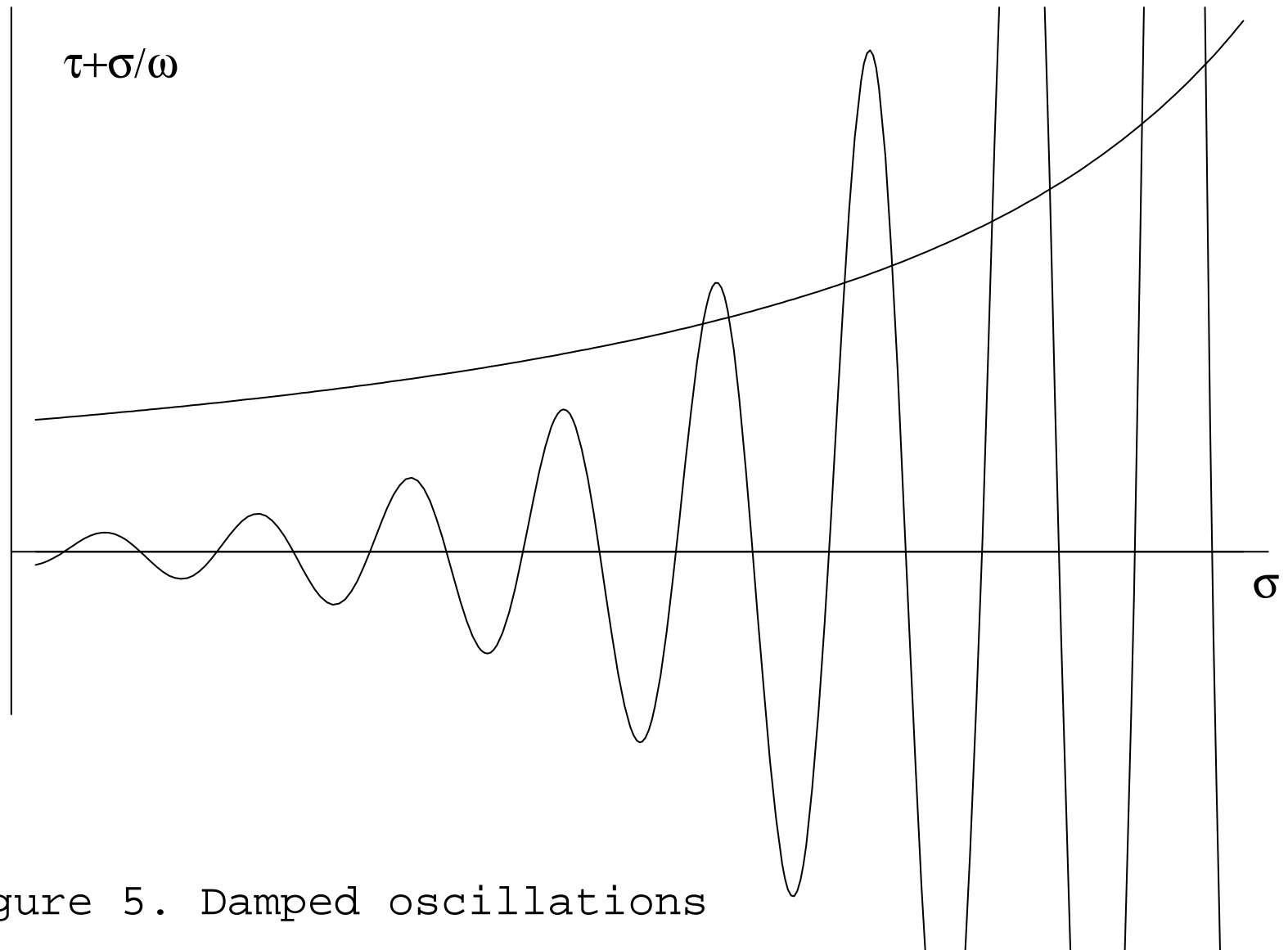


Figure 5. Damped oscillations
of $\Theta(\sigma)$ vs. constraint $2st=Z$